

Inference on 3D Procrustes Means: Tree Bole Growth, Rank Deficient Diffusion Tensors and Perturbation Models

Dedicated to the Memory of Herbert Ziezold (1942 – 2008)

Stephan Huckemann *

Abstract

The Central Limit Theorem (CLT) for extrinsic and intrinsic means on manifolds is extended to a generalization of Fréchet means. Examples are the Procrustes mean for 3D Kendall shapes as well as a mean introduced by Ziezold. This allows for one-sample tests previously not possible, and to numerically assess the ‘inconsistency of the Procrustes mean’ for a perturbation model and ‘inconsistency’ within a model recently proposed for diffusion tensor imaging. Also it is shown that the CLT can be extended to mildly rank deficient diffusion tensors. An application to forestry gives the temporal evolution of Douglas fir tree stems tending strongly towards cylinders at early ages and tending away with increased competition.

Key words and phrases: Kendall’s Shape Spaces, Central Limit Theorem, Bootstrap Confidence Intervals, Strong Consistency, Non-Parametric Inference, Ziezold Means, Forest Biometry, Tree-Stem Ellipticality

Figure *AMS 2000 Subject Classification:* Primary 62H11
Secondary 62G20, 62H15

1 Introduction

The study of descriptors of geometrical objects encompassed by terms of *form* or *shape* be it for artisanry, biological and morphological interest or medical applications dates back to the very origins of mankind. It took, and it still takes, however, until modern days to fully realize, that underlying most seemingly intuitive concepts of shape are rather counter-intuitive non-Euclidean geometries. Adding to counter-intuition, going from 2D to 3D shapes, these geometries cease to be well behaved. For this reason, the statistical analysis of 3D shapes is highly challenging and has gained much less attention in theory and practice.

*Supported by Deutsche Forschungsgemeinschaft Grant MU 1230/10-1 and DFG Graduate School 1023. Part of this research is contained in the habilitation thesis of the author.

This work has been motivated by a joint research with the Institute for Forest Biometry and Informatics at the University of Göttingen studying the temporal evolution of the 3D shape of tree boles over their growing periods. The task tackled here is to assess their growth towards and away from cylinders over time. This research is not only of interest in understanding fundamentals of biological growth and subsequent model building, cf. Skatter and Hoibo (1998); Koizumi and Hirai (2006). Also, the deviation from cylindricity has a direct economical impact by reducing log volume and increasing the number of turns to reposition logs for commercial sawing processes, cf. Rappold et al. (2007).

While Procrustes analysis is a well established tool for the statistical analysis of shape (e.g. Dryden and Mardia (1998) and Dryden (2009) for numerical routines), to the knowledge of the author, for 3D there are no asymptotic results available. Rather there is the belief that Procrustes sample means are unqualified for inference even in 2D because they may be “inconsistent estimators” of the “shape of the mean” – the latter being the mean of a *perturbation model* – unless the error is isotropically distributed, see Lele (1993), Kent and Mardia (1997) as well as Le (1998). This perturbation model introduced by Goodall (1991) and discussed in detail in Section 4 (cf. (4) on page 11), assumes error on the original configurations. The results cited above allowed inference based on Procrustes means only for a limited set of 2D scenarios, e.g. when randomness is caused by a procedure of acquiring landmarks independent of rotation and location. For more general settings as often occur in applications of biology, e.g. when randomness is also the result of non-uniform biological growth, however, Procrustes means could only contribute to data description while they were not considered for use in inferential statistics.

Such more general applications in mind, Bhattacharya and Patrangenaru (2003, 2005) established an asymptotic theory for *intrinsic* and *extrinsic* means on manifolds allowing for *non-parametric* asymptotic inference. Here “non-parametric” stands for the general approach not silently relying on a mean given by a perturbation model in the configuration space. Curiously in 2D, Procrustes means coincide with extrinsic means, the latter being “consistent” in the statistical sense i.e. satisfying a Strong Law of Large Numbers, see Ziezold (1977), Le (1998) as well as Bhattacharya and Patrangenaru (2003). Due to the dominating paradigm of the perturbation model, it seems that the notion of a Procrustes *population* mean has not quite found its way into the community.

Recently, a perturbation model has also motivated a non-standard approach in the context of neuro-imaging by Dryden et al. (2009b), employing Procrustes analysis for estimating a mean diffusion tensor. Although “perturbation consistency” has not been established, practical imaging results in particular for nearly degenerate tensors have been of very good quality.

It is the intention of this work to

- (a) make 3D Procrustes means with their well behaved asymptotics available for the practitioners in the field,
- (b) to provide for an assessment of “inconsistency” with perturbation models on Kendall’s shape spaces as well as for the approach of Dryden et al.

(2009a) for diffusion tensor imaging, and

- (c) to derive a framework to obtain the temporal shape motion relative to the shape of cylinders for a sample of Douglas fir tree stems.

To this end, the following Section 2 reviews Procrustes analysis and related results. Section 3 places Procrustes means and a mean introduced by Ziezold (1994) in the context of Fréchet means and gives the Central-Limit-Theorem (CLT) as the main theoretical result. Here, two aspects require special attention: first, a CLT can only hold on manifolds while in 3D, the underlying shape spaces cease to be that; secondly, since 3D Procrustes means are neither intrinsic nor extrinsic means, the CLT of Bhattacharya and Patrangenaru (2005) is accordingly modified as detailed in the appendix.

In Section 4 it is clarified that the reported “(in)consistency” of Procrustes means expresses “(in)compatibility” of a perturbation model with the canonical shape space geometry. Moreover for 3D, simulations based on the CLT show that for isotropic errors the perturbation model can be considered nearly compatible in most practical situations unless the shape of the perturbation mean is almost degenerate. In contrast by simulation in Section 5, a similar perturbation model for mean diffusion tensors is not compatible, not even for small isotropic errors. Curiously, however, with increased degeneracy of the perturbation mean considered, incompatibility seems not increasing. This is also the case for an extension of the model to *mildly rank deficient* diffusion tensors, presented here.

Section 6 introduces a framework for the assessment of shape of frusta cut from tree boles. It turns out that the shapes of cylinders form a geodesic in the shape space allowing for the computation of the distance of arbitrary frusta to the space of cylinders. For statistical inference, Bootstrap confidence intervals for this distance are simulated from a sample of reconstructed tree ring structures of small size. Comparison with two typical growth scenarios gives that the bole shape of young trees with little competition grows uniformly or stronger towards cylinders, while the motion of shapes of old tree boles with heavy competition away from cylinders is similar to a growth maintaining cross-sectional ellipticality and tapering.

2 Procrustes Analysis and Kendall’s Shape Spaces

In the statistical analysis of similarity shapes based on landmark configurations, geometrical m -dimensional objects (usually $m = 2, 3$) are studied by placing $k > m$ *landmarks* at specific locations of each object. Each object is then described by a matrix in the space $M(m, k)$ of $m \times k$ matrices, each of the k columns denoting an m -dimensional landmark vector. $\langle x, y \rangle := \text{tr}(xy^T)$ denotes the usual inner product with norm $\|x\| = \sqrt{\langle x, x \rangle}$. For convenience and without loss of generality for the considerations below, only *centered* configurations are considered. Centering in way treating all landmarks equally can be achieved by multiplying with a sub-Helmert matrix \mathcal{H}

$$\mathcal{H} = \begin{pmatrix} \frac{1}{\sqrt{2}} & \frac{1}{\sqrt{6}} & \cdots & \frac{1}{\sqrt{k(k-1)}} \\ -\frac{1}{\sqrt{2}} & \frac{1}{\sqrt{6}} & \cdots & \frac{1}{\sqrt{k(k-1)}} \\ 0 & -\frac{2}{\sqrt{6}} & \cdots & \frac{1}{\sqrt{k(k-1)}} \\ \vdots & \vdots & \ddots & \vdots \\ 0 & 0 & \cdots & -\frac{k-1}{\sqrt{k(k-1)}} \end{pmatrix} \in M(k, k-1) \quad (1)$$

from the right, yielding $x\mathcal{H}$ in $M(m, k-1)$. This corresponds to the relocating of objects in space such that their mean landmark is zero and isometrically projecting the linear sub space of matrices with vanishing mean landmark to the space of matrices with $k-1$ of landmarks. For this method and other centering methods cf. Dryden and Mardia (1998, Chapter 2). Excluding also all matrices with all landmarks coinciding gives the space of *configurations*

$$F_m^k := M(m, k-1) \setminus \{0\}.$$

Since only the similarity shape is of concern, all configurations are considered modulo the group of similarity transformations $H = SO(m) \times \mathbb{R}_+$ (recall that we excluded w.l.o.g. translations) where the action is given by the operation $(g, \lambda)x = g\lambda x$. Here, $SO(m)$ denotes the special orthogonal group (the orientation preserving orthogonal transformations). The *shape* of a configuration $x \in F_m^k$ is the orbit $[x] = \{hx : h \in H\}$, the *shape space* is the quotient $F_m^k/H = \{[x] : x \in F_m^k\}$ with a suitable metric.

A naïve shape space. A straightforward metric structure for F_m^k/H is given by the canonical quotient metric:

$$\inf_{h_1, h_2 \in H} \|h_1 x_1 - h_2 x_2\| \text{ for } x_1, x_2 \in F_m^k.$$

Unfortunately, due to the scaling action of \mathbb{R}_+ , this metric is identically zero, a dead end for statistical ambition.

General Procrustes analysis (GPA). As a workaround, Gower (1975) introduced a constraining condition which allowed for the definition of a mean. For a sample of configurations $x_1, \dots, x_n \in F_m^k$ a *full Procrustes sample mean* is given by the shape of

$$\frac{1}{n} \sum_{j=1}^n h_j^* x_j$$

where h_1^*, \dots, h_n^* are minimizers over $h_1, \dots, h_n \in H$ of the *Procrustes sum of squares*

$$\sum_{i,j=1}^n \|h_j x_j - h_i x_i\|^2 \text{ under the constraining condition } \left\| \frac{1}{n} \sum_{j=1}^n h_j x_j \right\| = 1.$$

Letting $\mu = \frac{1}{n} \sum_{j=1}^n h_j x_j$, $h_j = (g_j, \lambda_j)$, the Procrustes sum of squares is

$$\sum_{i,j=1}^n \|h_j x_j - h_i x_i\|^2 = 2n \sum_{j=1}^n \|h_j x_j - \mu\|^2 = 2n \sum_{j=1}^n \|\lambda_j g_j x_j - \mu\|^2.$$

W.l.o.g. we may assume that all configurations are contained in the unit sphere

$$S_m^k := \{x \in M(m, k-1) : \|x\| = 1\}.$$

Then, any minimizing μ is the orthogonal projection of the mean of minimizing $h_1 x_1, \dots, h_n x_n$ to S_m^k . In consequence, minimization can be performed sequentially, first for the λ_j , then for the g_j and finally for μ , as noted. Partial differentiation in particular gives the minimizing $\lambda_j^* = \langle g_j x_j, \mu \rangle > 0$ (unless $\langle g x_j, \mu \rangle = 0$ for all $g \in SO(m)$) such that every μ^* having the shape of a full Procrustes sample mean is a minimizer of

$$\min_{\mu \in S_m^k} \min_{\substack{g_1, \dots, g_n \in SO(m) \\ \langle g_i x_i, \mu \rangle \geq 0, i = 1, \dots, n}} \sum_{j=1}^n \|\langle g_j x_j, \mu \rangle g_j x_j - \mu\|^2 = \min_{\mu \in S_m^k} \sum_{j=1}^n \delta(x_j, \mu)^2$$

with the *residual distance*

$$\delta(x, y) := \min_{\substack{g \in SO(m) \\ \langle gx, y \rangle \geq 0}} \|\langle gx, y \rangle gx - y\|. \quad (2)$$

Kendall's shape spaces. Kendall (1977) proposed a slightly different work-around. Instead of considering the quotient w.r.t. the action of \mathbb{R}_+ , he projected all configurations to S_m^k called the *pre-shape sphere* and considered the metric quotient w.r.t. $SO(m)$ only, which is called *Kendall's shape space*

$$\Sigma_m^k := S_m^k / SO(m) = \{[x] : x \in S_m^k\} \text{ with the fiber } [x] = \{gx : g \in SO(m)\}.$$

Kendall's shape space is thus a quotient of a sphere allowing for two non-trivial canonical quotient metrics

$$d_{\Sigma_m^k}([x], [y]) := \inf_{g, h \in SO(m)} d(gx, hy) = \inf_{g \in SO(m)} d(gx, y),$$

d denoting either the Euclidean distance on F_m^k or the *spherical* distance on S_m^k :

$$d_{F_m^k}^{(e)}(x, y) := \|x - y\|, \quad d_{S_m^k}^{(s)}(x, y) := 2 \arcsin \frac{\|x - y\|}{2}.$$

In some applications only the *form*, i.e. shape without size filtered out is of interest. The corresponding *size-and-shape space* is $S\Sigma_m^k := F_m^k / SO(m)$ with *size-and-shape* $[x] := \{gx : g \in SO(m)\} \in S\Sigma_m^k$ of $x \in F_m^k$. For a sample $x_1, \dots, x_n \in F_m^k$, *partial Procrustes sample means*, the size-and-shapes of $\mu^* \in F_m^k$ are then considered which minimize

$$\min_{g_1, \dots, g_n \in SO(m)} \sum_{j=1}^n \|\mu - g_j x_j\|$$

over $\mu \in F_m^k$. Obviously, $\mu^* = \frac{1}{n} \sum_{j=1}^n g_j^* x_j$ with minimizers $g_1^*, \dots, g_n^* \in SO(m)$. These means are “partial” because no equivalence w.r.t. scaling is considered. In contrast, in the definition of full Procrustes means above equivalence under the full group of similarities is considered.

2D full Procrustes means are extrinsic means. For $m = 2$, Kendall (1984) observed that one may identify F_2^k with $\mathbb{C}^{k-1} \setminus \{0\}$ such that every landmark column corresponds to a complex number. This means in particular that $z \in \mathbb{C}^{k-1}$ is a complex row-vector. With the Hermitian conjugate $a^* = (\overline{a_{kj}})$ of a complex matrix $a = (a_{jk})$ the pre-shape sphere S_2^k is identified with $\{z \in \mathbb{C}^{k-1} : zz^* = 1\}$ on which $SO(2)$ identified with $S^1 = \{\lambda \in \mathbb{C} : |\lambda| = 1\}$ acts by complex scalar multiplication. Then the well known Hopf-Fibration gives $\Sigma_2^k = S_2^k / S^1 = \mathbb{C}P^{k-2}$, the complex projective $(k-2)$ -dimensional space. Moreover, denoting by $M(k-1, k-1, \mathbb{C})$ all complex $(k-1) \times (k-1)$ matrices, the *Veronese-Whitney embedding* is given by

$$\mathbf{v} : \Sigma_2^k \rightarrow \{a \in M(k-1, k-1, \mathbb{C}) : a^* = a\}, \quad [z] \mapsto z^* z.$$

If $Z \in \mathbb{C}^{k-1}$ is a random pre-shape, identifying $\mathbf{v}(\Sigma_2^k)$ with Σ_2^k , the set of *extrinsic means* (cf. Bhattacharya and Patrangenaru (2003)) of $[Z]$ is the set of shapes of the orthogonal projection of the usual expected value $\mathbb{E}(Z^* Z)$ to $\mathbf{v}(\Sigma_2^k)$. Employing complex linear algebra, the set of extrinsic means is easily identified as the shapes of the eigenvectors to the largest eigenvalue of the *complex integral of squares matrix* $\mathbb{E}(Z^* Z)$. Since on the other hand

$$\mathbb{E}(\delta(Z, w)^2) = 1 - w \mathbb{E}(Z^* Z) w^*.$$

with the residual shape distance from (2), we have that that any eigenvector of $\mathbb{E}(Z^* Z)$ to its largest eigenvalue is a pre-shape of a full Procrustes mean.

Theorem 2.1. *The set of 2D full Procrustes means is the inverse image under the Veronese-Whitney embedding of the set of extrinsic means on $\mathbf{v}(\Sigma_2^k)$.*

In most applications, the largest eigenvalue of $\mathbb{E}(Z^* Z)$ is simple, then the 2D full Procrustes mean is uniquely determined.

A similar procedure gives extrinsic means using the *Schoenberg embedding* for the related space of Kendall’s *reflection shapes* of arbitrary dimension, not discussed here, cf. Bhattacharya (2008). Procrustes means for three- and higher-dimensional configurations, however, cannot be modeled in this vein.

3 Asymptotics for Procrustes and Ziezold Means

In this section we will see that 3D and higher-dimensional Procrustes means as well as a mean introduced by Ziezold (1994) are special cases of Fréchet ρ -means. In the following, *smooth* means at least twice continuously differentiable.

3.1 Kendall's Higher-dimensional Shape Spaces

As we have seen above, Σ_2^k is a manifold, namely a complex projective space. Similarly, $S\Sigma_2^m$ can be given a manifold structure. For $m \geq 3$, however, Σ_m^k and $S\Sigma_m^k$ cease to be manifolds, they only contain dense and open submanifolds

$$\begin{aligned} (\Sigma_m^k)^* &:= (S_m^k)^*/SO(m) & \text{with } (S_m^k)^* &:= \{x \in S_m^k : \text{rank}(x) \geq m-1\} \\ (S\Sigma_m^k)^* &:= (F_m^k)^*/SO(m) & \text{with } (F_m^k)^* &:= \{x \in F_m^k : \text{rank}(x) \geq m-1\} \end{aligned}$$

called the *manifold parts* of *regular* or equivalently *non-degenerate* shapes, size-and-shapes, pre-shapes and configurations, respectively. A pre-shape or configuration x or its shape or its size-and-shape $[x]$ is called *strictly regular* if $\text{rank}(x) = m$. In case of Σ_m^k , $m \geq 3$, approaching degenerate shapes, some sectional curvatures are unbound. A detailed discussion can be found in Kendall et al. (1999) as well as Huckemann et al. (2010).

Note that the square of a distance may not be smooth at so called cut points. E.g the square of the spherical distance between e^{it} and e^{is} on the unit circle $S^1 \subset \mathbb{C}$ is smooth except when $e^{i(t-s)} = -1$. In general on a Riemannian manifold, the *cut locus* $C(p)$ of p comprises all points q such that the extension of a length minimizing geodesic joining p with q is no longer minimizing beyond q . If $q \in C(p)$ or $p \in C(q)$ then p and q are *cut points*.

Lemma and Definition 3.1. *All of*

$$\begin{aligned} d_{\Sigma_m^k}^{(i)}([x], [y]) &:= \min_{g \in SO(m)} d_{S_m^k}^{(s)}(gx, y), \\ d_{\Sigma_m^k}^{(p)}([x], [y]) &:= \sin d_{\Sigma_m^k}^{(i)}([x], [y]) = \min_{\substack{g \in SO(m) \\ \langle gx, y \rangle \geq 0}} \sqrt{1 - \langle gx, y \rangle^2}, \\ d_{\Sigma_m^k}^{(z)}([x], [y]) &:= 2 \sin \frac{d_{\Sigma_m^k}^{(i)}([x], [y])}{2} = \min_{g \in SO(m)} \sqrt{2(1 - \langle gx, y \rangle)}, \\ d_{S\Sigma_m^k}^{(i)}([x], [y]) &:= \min_{g \in SO(m)} d_{F_m^k}^{(e)}(gx, y) = \min_{g \in SO(m)} \sqrt{\|x\|^2 + \|y\|^2 - 2\langle gx, y \rangle} \end{aligned}$$

are metrics on the shape space and the size-and-shape space, respectively, and their squares are smooth on the respective manifold parts except at cut points.

Proof. If the canonical quotient $Q = M/G$ of a smooth Riemannian manifold M due to the action of a Lie group $G = SO(m)$ on M is a Riemannian manifold, then the intrinsic distance on Q is a smooth metric (cf. Abraham and Marsden (1978, Chapter 4.1)). This gives the smoothness of $(d^{(i)})^2$ on the respective manifold parts which are dense in the shape space and the size-and-shape space, respectively, except at cut points. Hence, the $d^{(i)}$ extend to metrics on these. Moreover, $d_{\Sigma_m^k}^{(z)}$ is a metric due to convexity and monotonicity of $t \rightarrow 2 \sin(t/2)$ for $t \in [0, \pi]$; for $d_{\Sigma_m^k}^{(p)}$ we rely on Kendall et al. (1999, p. 206). \square

We say that x is in *optimal position* to y if $\max_{g \in SO(m)} \langle gx, y \rangle = \langle x, y \rangle$. In particular then $d_{\Sigma_m^k}^{(z)}([x], [y]) = \|x - y\|$ and $d_{S\Sigma_m^k}^{(i)}([x], [y]) = \|x - y\|$, respectively.

3.2 Fréchet ρ -Means

The Central-Limit-Theorem (CLT) derived below relies on the “ δ -method” for smooth transformations. In consequence, we can only expect a CLT theorem

to hold on the manifold part of the shape space and the size-and-shape space, respectively. For the following we assume that (Q, d) is a metric space and P is a D -dimensional smooth Riemannian manifold. For example, $Q = \Sigma_m^k$ and $P = (\Sigma_m^k)^*$. Suppose that X, X_1, X_2, \dots are i.i.d. random variables mapping from an abstract probability space $(\Omega, \mathcal{A}, \mathbb{P})$ to Q equipped with its Borel σ -field. For a random vector $Y \in \mathbb{R}^D$, $\mathbb{E}(Y)$ denotes the usual expectation, if defined.

Definition 3.2. For a continuous function $\rho : Q \times P \rightarrow [0, \infty)$ define the set of population Fréchet ρ -means of X in P by

$$E^{(\rho)}(X) = \operatorname{argmin}_{\mu \in P} \mathbb{E}(\rho(X, \mu)^2).$$

For $\omega \in \Omega$ denote the set of sample Fréchet ρ -means by

$$E_n^{(\rho)}(\omega) = \operatorname{argmin}_{\mu \in P} \sum_{j=1}^n \rho(X_j(\omega), \mu)^2.$$

Since their original definition by Fréchet (1948) for $P = Q$ and $\rho = d$, such means have found much interest. Ziezold (1977) extended the concept to ρ being a quasi-metric only. On Riemannian manifolds ($Q = P$) w.r.t. the Riemannian metric ρ , Bhattacharya and Patrangenaru (2003, 2005) introduced the corresponding means as *intrinsic means*, and, taking ρ to be the metric of an ambient Euclidean space, as *extrinsic means*.

In consequence of Lemma and Def. 3.1 and the connection with the residual distance (2), $d_{\Sigma_m^k}^{(p)}([x], [y]) = \delta(x, y)$, we can at once identify Procrustes means.

Corollary 3.3. The set of ρ -Fréchet sample means on the shape space and size-and-shape space, respectively, are the sets of

- (i) full Procrustes sample means for $\rho = d_{\Sigma_m^k}^{(p)}$,
- (ii) partial Procrustes sample means for $\rho = d_{S\Sigma_m^k}^{(i)}$.

For $m = 2$, Ziezold (1994) introduced mean shapes w.r.t. $\rho = d_{\Sigma_m^k}^{(z)}$ which have been studied also by Le (1998). The following first two definitions honor his memory. The other extend sample Procrustes means to the population case.

Definition 3.4. Call $d_{\Sigma_m^k}^{(z)}$ the Ziezold metric on the shape space, and the Fréchet $d_{\Sigma_m^k}^{(z)}$ -means the set of Ziezold means. The Fréchet $d_{\Sigma_m^k}^{(p)}$ -means are the set of full Procrustes means, the Fréchet $d_{S\Sigma_m^k}^{(i)}$ -means the set of partial Procrustes means.

Ziezold means and full Procrustes means, even though defined earlier, can be thought of as a generalization of extrinsic means and means for crude residuals (cf. Mardia and Jupp (2000)), respectively. Partial Procrustes means are extensions of intrinsic means to non-manifolds.

Let us now touch on the issues of existence and uniqueness for the above introduced means. Both are rather simple issues for extrinsic means, since

they are orthogonal projections of classical Euclidean means in an ambient space to the embedded manifold in question, this projection being well defined except for a set of Lebesgue measure zero (cf. Bhattacharya and Patrangenaru (2003)). For non-extrinsic means as above, however, existence, namely that the means are assumed on the manifold part is a deeper issue tackled in Huckemann (2010). Intrinsic means are unique if the underlying random elements are sufficiently concentrated (cf. Le (2001) for the elaborate proof). For higher-dimensional Ziezold and full Procrustes means, to the knowledge of the author, there are no uniqueness results available.

Since we are concerned with metrics, the following is a consequence of the Strong Law by Ziezold (1977), cf. also Bhattacharya and Patrangenaru (2003).

Theorem 3.5. *Suppose that X is a random pre-shape in S_m^k or a random configuration in F_m^k with unique Ziezold, full Procrustes or partial Procrustes mean $[\mu]$. Then every measurable selection $[\mu_n(\omega)]$ from the sets of sample Ziezold, full Procrustes or partial Procrustes means, respectively, is a strongly consistent estimator of $[\mu]$.*

For the following we need the condition that $[X]$ is bounded away from the cut locus of the mean a.s. in the Ziezold or full/partial Procrustes sense

$$\exists \epsilon > 0 \quad \text{such that} \quad d([X], [\mu]) < d(C([\mu]), [\mu]) - \epsilon \quad \text{a.s.} \quad (3)$$

where $[\mu]$ and d are corresponding Ziezold, full Procrustes or partial Procrustes means and distances, respectively.

3.3 The Central-Limit-Theorem

The Central-Limit-Theorem for Fréchet ρ -means requires additional setup.

Definition 3.6. *Let P be a D -dimensional manifold. We say that a P -valued estimator $\mu_n(\omega)$ of $\mu \in P$ satisfies a Central-Limit-Theorem (CLT), if in any local chart (ϕ, U) near $\mu = \phi^{-1}(0)$ there are a suitable $D \times D$ matrix A_ϕ and a Gaussian $D \times D$ matrix \mathcal{G}_ϕ with zero mean and semi-definite symmetric covariance matrix Σ_ϕ such that*

$$\sqrt{n}A_\phi(\phi(\mu_n) - \phi(\mu)) \rightarrow \mathcal{G}_\phi$$

in distribution as $n \rightarrow \infty$.

In most applications A_ϕ is non-singular, then in consequence of the “ δ -method”, for any other chart (ϕ', U) near $\mu = \phi'^{-1}(0)$ we have simply

$$A_{\phi'}^{-1}\Sigma_{\phi'}(A_{\phi'}^{-1})^T = J(\phi' \circ \phi^{-1})_0 A_\phi^{-1}\Sigma_\phi(A_\phi^{-1})^T J(\phi' \circ \phi^{-1})_0^T$$

where $J(\cdot)_0$ denotes the Jacobian matrix of first derivatives at the origin.

In consequence of Theorem 3.5 and Theorem A.1 from the appendix (assertion (ii) follows from Bhattacharya and Patrangenaru (2005)) we have the following.

Theorem 3.7. *Suppose that X is a random pre-shape in S_m^k or a random configuration in F_m^k , $[X]$ having a unique Ziezold, full Procrustes or partial Procrustes mean $[\mu]$ on the respective manifold part. Then every measurable selection $[\mu_n(\omega)]$ from the sets of sample Ziezold, full Procrustes or partial Procrustes means, respectively, satisfies a Central-Limit-Theorem if $[X]$ is bounded away from the cut locus of the mean a.s. in the Ziezold or full/partial Procrustes sense (3) under the following additional condition:*

- (i) none in case of Ziezold or full Procrustes means,
- (ii) in case of partial Procrustes means, if the Euclidean second moment $\mathbb{E}(\|X\|^2)$ is finite.

In a suitable chart (ϕ, U) the corresponding matrices from Definition 3.6 are given by

$$A_\phi = \mathbb{E}(H\rho([X], [\mu])), \quad \Sigma_\phi = \text{COV}(\text{grad } \rho([X], [\mu]))$$

where ρ denotes the distances $d_{\Sigma_m^k}^{(p)}$, $d_{\Sigma_m^k}^{(z)}$ and $d_{S\Sigma_m^k}^{(i)}$, respectively. Moreover, grad and H denote the gradient and Hessian of $x \mapsto \rho([X], [\phi^{-1}(x)])^2$, respectively.

Numerical simulations show a rather good finite sample accuracy of the CLT, cf. Figure 1.

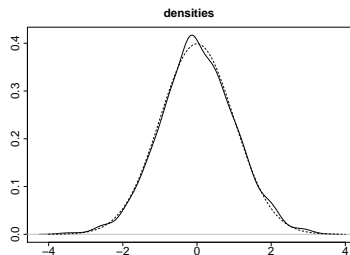


Figure 1: *Depicting the proximity to the standard normal density (dashed line) of the normalized density (solid line) of the non-zero coordinate of full Procrustes means of samples of size $n = 10$ from the geodesic perturbation model (9) in Σ_3^4 with $\epsilon_i = 0$ and $s_i \sim N(0, 0.1^2)$ with the two-dimensional mean $\mu = \text{diag}(1, -1, 0)/\sqrt{2}\mathcal{H}^T$ and $\nu = \text{diag}(1, 1, 1)/\sqrt{3}\mathcal{H}^T$.*

Remark 3.8. *For $m \geq 3$, computing Ziezold means (for an algorithm cf. Ziezold (1994)) is computationally less costly than computing full Procrustes means (corresponding algorithms are discussed in Dryden and Mardia (1998, Chapter 5.3)): for full Procrustes means in every iteration step every single optimal positioned datum needs additionally to be projected to the tangent space. The simulations reported in Section 4.1 and the Bootstrap simulations in Section 6 give similar results but are approximately 15% faster when using Ziezold means instead of full Procrustes means.*

Remark 3.9. *Grossier (2005) proves that the above algorithms converge under rather broad conditions and supplies error estimates.*

4 Perturbation Inconsistency for Kendall Shapes

For brevity in this section unless otherwise specified, Procrustes means refer to full Procrustes means.

Goodall (1991) proposed to model a sample of landmark configuration matrices y_i ($i = 1, \dots, n$) with a *perturbation model* that since then, has been highly popular in the community:

$$y_i = \lambda_i g_i(\mu + \epsilon_i) + t_i. \quad (4)$$

The $\lambda_i > 0$ convey scaling, the g_i are rotation matrices and the t_i stand for translations. Obviously, these three sets of nuisance parameters keep the *shape* invariant, of interest is only the deterministic *perturbation mean* μ and the random perturbations ϵ_i with zero expectation. If the size is also of interest then set $\lambda_i = 1$ keeping only the form invariant under rotation and translation. Under the assumption of isotropic Gaussian errors ϵ_i , for estimation and inference on the population perturbation means μ_i and error covariances ϵ_i , Goodall (1991) proposed to use *sample Procrustes means* obtained from GPA, cf. Section 2. In the sequel, the property that (for arbitrary errors) sample Procrustes means converge to the shape of the mean of an underlying perturbation model has been coined as the “consistency of Procrustes means”.

4.1 Isotropic 3D Error

In order to validate Goodall’s proposal, Kent and Mardia (1997) studied the analog of the perturbation model (4) on the pre-shape sphere and showed that for 2D configurations with isotropic ϵ_i , the Procrustes population mean from (4) is identical with the shape of the perturbation mean. Le (1998) extended these results and showed that under slightly relaxed conditions for 2D configurations, intrinsic, Ziezold and Procrustes means all agree with the shape of μ .

For 3D shapes the above arguments are no longer valid because the shape-fibres in S_m^k are not spanned by geodesics in general (see Huckemann et al. (2010, Example 5.1)), hence equality of Procrustes means with the shape of a perturbation model cannot be expected, even for very small isotropic error.

In order to assess the practical impact of this effect, we measure the distance between the shape of the perturbation mean and its corresponding Procrustes mean. In view of Theorem 3.7, this can be done by determining the distance between the shape of the perturbation mean and a corresponding sampled Procrustes mean while confidence or equivalently its accuracy can be estimated by distances of correspondingly sampled sample Procrustes means to their sample Procrustes mean. The following considerations detail this setup.

Consider a random $X = Y\mathcal{H}/\|Y\mathcal{H}\| \in S_m^k$ with Y from a perturbation model (4) such that the following means are unique. Assume $\mu \in S_m^k$ and denote by

ν the pre-shape of the Procrustes population mean in optimal position to μ ;

$\hat{\nu}^{(n)}$ the random pre-shape in optimal position to ν of the Procrustes sample mean of X_1, \dots, X_n i.i.d. as X ;

$\mu\mathcal{H}$	σ	$\hat{d}^{(n,N)}$	$\hat{\sigma}^{(n,N)}$
$\frac{1}{\sqrt{3}} \begin{pmatrix} 1 & 0 & 0 \\ 0 & 1 & 0 \\ 0 & 0 & 1 \end{pmatrix}$	0.5	0.011	0.0097
	0.1	0.0023	0.0021
	0.01	0.00022	0.00020
$\frac{1}{\sqrt{1.1}} \begin{pmatrix} 1 & 0 & 0 \\ 0 & 0.3 & 0 \\ 0 & 0 & 0.1 \end{pmatrix}$	0.5	0.30	0.030
	0.1	0.016	0.0022
	0.01	0.00026	0.00020
$\frac{1}{\sqrt{1.001}} \begin{pmatrix} 1 & 0 & 0 \\ 0 & 0.01 & 0 \\ 0 & 0 & 0 \end{pmatrix}$	0.1	0.12	0.082
	0.01	0.0055	0.00044
	0.001	$5.0e - 05$	$2.0 - 05$

Table 1: Estimated distance $\hat{d}^{(n,N)}$ between shape of the mean μ of the perturbation model (4) and corresponding Procrustes mean with standard error $\hat{\sigma}^{(n,N)}$ for $n = 10,000$ and $N = 10$. The error follows independently $\mathcal{N}(0, \sigma^2)$ in every component. For convenience the Helmertized pre-shape $\mu\mathcal{H}$ is reported displaying proximity to degeneracy.

$\hat{\nu}_j^{(n)}$ for $j = 1, \dots, N$ i.i.d. realizations of $\hat{\nu}^{(n)}$,

$\hat{\nu}^{(n,N)}$ a realization of the Procrustes sample mean of $\hat{\nu}_1^{(n)}, \dots, \hat{\nu}_N^{(n)}$ in optimal position to ν .

Then in consequence of Theorem 3.7,

$$\hat{\sigma}^{(n,N)} := \sqrt{\frac{1}{N} \sum_{j=1}^N d_{\Sigma_m^k}^{(p)}([\hat{\nu}_j^{(n)}], [\hat{\nu}^{(n,N)}])^2} \approx \sqrt{\mathbb{E}(d_{\Sigma_m^k}^{(p)}([\hat{\nu}^{(n)}], [\nu])^2)}$$

gives an approximation of the confidence into or accuracy of the measurement of ν by $\hat{\nu}^{(n)}$. On the other hand, we have the approximation

$$\hat{d}^{(n,N)} := \sqrt{\frac{1}{N} \sum_{j=1}^N d_{\Sigma_m^k}^{(p)}([\nu_j^{(n)}], [\mu])^2} \approx \sqrt{\mathbb{E}(d_{\Sigma_m^k}^{(p)}(\nu^{(n)}, \mu)^2)}.$$

The goodness of both approximations depends on N . Moreover for fixed N , $\hat{\sigma}^{(n,N)}$ can be made arbitrarily small by choosing n sufficiently large. If alongside, $\hat{d}^{(n,N)}$ also becomes equally small, this can be taken as strong evidence that the shape of the perturbation model agrees with the corresponding Procrustes mean. Otherwise, we have strong evidence, that the two disagree. Table 1 reports values of $\hat{d}^{(n,N)}$ and $\hat{\sigma}^{(n,N)}$ for typical simulations of (4) for $m = 3, k = 4$ with isotropic i.i.d Gaussian error ϵ of variance σ^2 . The following remark summarizes the results of these and further simulations.

Remark 4.1. *In approximation the perturbation model (4) with isotropic errors is compatible with the geometry of Σ_3^k if the perturbation mean is far from degenerate. For nearly degenerate perturbation means, however, the perturbation model may be incompatible even for small isotropic errors. Using Ziezold means instead of Procrustes means gives similar results.*

4.2 Non-Isotropic 2D Error

Global effects. Recall from Section 2, modeling Σ_2^k by a complex projective space. Since the eigenvectors of the complex integral of squares matrix may vary discontinuously under continuous matrix variation this led Kent and Mardia (1997) to the conclusion that Procrustes means can be inconsistent where in fact they are statistically consistent but possibly discontinuous.

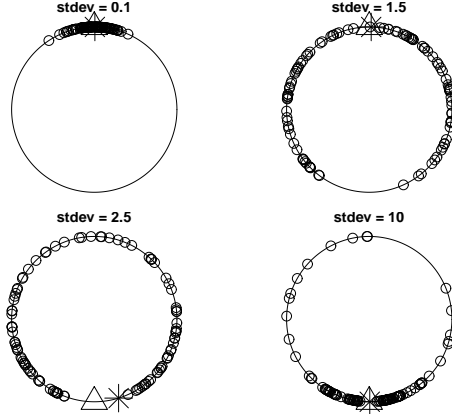


Figure 2: Great circle in Σ_2^3 spanned by the shapes of the perturbation (5). The little circles denote 100 sampled shapes, the star their Procrustes sample mean and the triangle the respective Procrustes population mean. The respective headers give the standard deviation of the Gaussian ϵ .

In view of the perturbation model (4) consider in the spirit of Kent and Mardia (1997, p. 285) the complex configuration $\mu = (\sqrt{2}, 0, 1/\sqrt{2}) \in \mathbb{C}^3$ additively perturbed by the non-isotropic random $\epsilon = (0, 0, \sqrt{6}\eta t/2) \in \mathbb{C}^3$, $t \sim \mathcal{N}(0, 1)$, $\eta > 0$, modeling linear configurations with two fixed endpoints and a random landmark varying in the middle. The Kendall pre-shape of

$$\mu + \epsilon \tag{5}$$

is given by $z = \frac{1}{\sqrt{1+\eta^2 t^2}}(1, \eta t)$ with the complex integral of squares matrix

$$\begin{pmatrix} \mathbb{E}\left(\frac{1}{1+\eta^2 t^2}\right) & 0 \\ 0 & \eta^2 \mathbb{E}\left(\frac{t^2}{1+\eta^2 t^2}\right) \end{pmatrix}.$$

For small error intensity η , the shape of μ gives the Procrustes population mean. For higher error intensity, however, the Procrustes population mean indeed changes abruptly to the shape of the configuration $\nu = (\sqrt{2}, \sqrt{2}, -2\sqrt{2})$.

In order to visualize the situation in the shape space recall the Hopf fibration

$$S_2^3 \rightarrow \Sigma_2^3 = \mathbb{C}P^1 : (\alpha_1, \alpha_2) \mapsto \left(\operatorname{Re}(\alpha_1 \bar{\alpha}_2), \operatorname{Im}(\alpha_1 \bar{\alpha}_2), \frac{|\alpha_1|^2 - |\alpha_2|^2}{2} \right)$$

mapping from a three-sphere to a two-sphere. The counter-intuitive behavior of discontinuity of the Procrustes mean is visualized in Figure 2. As is clearly visible, the discontinuity of the Procrustes mean in the error's standard deviation

$\sqrt{6}\eta/2$ is due to the fact, that the corresponding shapes move along a common great circle in Σ_2^3 , from clustering at the top (the shape of μ) to clustering at the bottom (the shape of ν). The discontinuity observed by Kent and Mardia (1997) thus reflects a global effect of an “incompatibility” of the perturbation model with the geometry of the shape space.

Local effects. As above, Lele (1993, Figure 3 on p. 598) considers an example of a distribution of planar but now quadrangular configurations along a straight line in the configuration space F_2^4 . For simplicity of the argument consider $\mu = (i, 1, -i, -1)$, $\epsilon = (0, i, 0, -i)$ and the sample $z_1 = \mu + \epsilon$, $z_2 = \mu - \epsilon$, $\epsilon > 0$, with mean μ in Euclidean F_2^4 . One verifies immediately that z_1 and z_2 are not in optimal position, rather $\lambda = \frac{1}{\sqrt{5}}(1 + 2i)$ puts z_1 into optimal position λz_1 to z_2 w.r.t. to the action of $SO(2)$. Then the form of $(\lambda z_1 + z_2)/2$ is the partial Procrustes mean, which is different from the form of μ . The alleged “inconsistency” of the partial Procrustes mean is now a local effect of an “incompatibility” of the perturbation model with the canonical geometry of the size-and-shape space $S\Sigma_2^4$.

5 Asymptotics for Diffusion Tensors

In diffusion tensor neuro-imaging (for a short introduction into this young field, e.g. Vilanova et al. (2006)), the dominating eigenvector of a symmetric semi-positive definite (SPD) matrix from the space $P(m) = \{0 \neq a \in M(m, m) : a^T = a \geq 0\}$ exhibits the dominating direction of molecular displacement due to a flow in tissue fibres of interest. The statistical and non-statistical literature to the task of reconstructing SPD matrices which are called *diffusion tensors* (DTs) in this context is vast. Recently, matching techniques involving shape analysis (e.g. Cao et al. (2006)) have gained momentum.

A non-standard statistical approach to reconstruct a mean DT from an observed sample of neighboring DTs based on Procrustes methods has been proposed by Dryden et al. (2009b). One motivation comes from perturbation models, which, as it turns out below are “inconsistent” with Procrustes means. Coming as a surprise, however, practical image reconstructions based on this method in particular for nearly degenerate DTs, have produced results of convincingly good quality, cf. Dryden et al. (2009a). In the following, this approach is first extended to *mildly rank-deficient DTs* and secondly, perturbation inconsistency is assessed. Even though in most applications to imaging, the flow is observed in 2D or 3D, i.e. $m = 2, 3$, the following applies to arbitrary $m \in \mathbb{N}$.

Diffusion tensors observed in the “real world” fall into the sub-space $P^+(m) = \{a \in P(m) : a > 0\}$ of symmetric strictly positive definite matrices. This space – even though much more complicated than complex projective space – has been well studied (as the “universal symmetric space of non-compact type with non-positive non-constant sectional curvatures” e.g. Lang (1999, Chapter XII)).

Via the well known *Cholesky factorization*

$$\text{chol} : P^+(m) \rightarrow UT^+(m),$$

this space can equivalently be modelled by the group of m -dimensional upper triangular matrices $UT^+(m)$ with positive diagonal. Traditionally diffusion tensors have been modelled within these spaces, statistical analysis has either been carried out by using the extrinsic distance inherited from $M(m, m)$ (e.g. Pajevic and Basser (2003)) or the intrinsic distance due to the aforementioned structure (cf. Fletcher and Joshi (2004)). Modeling flow in ideal micro-fibres, obviously leads to rank-deficient diffusion tensors, which, however, are not contained in these manifolds. Unless one utilizes a Euclidean embedding e.g. in the space of symmetric matrices, a new structure has to be found.

5.1 A CLT for Mildly Rank-deficient Diffusion Tensors

Here, an embedding $P(m) \hookrightarrow \Sigma_m^{m+1}$ is proposed, that maps the space

$$P^*(m) = \{a \in P(m) : \text{rank}(a) \geq m - 1\}$$

of *mildly rank-deficient diffusion tensors* into the manifold part $(\Sigma_m^{m+1})^*$. This embedding is inspired by recent work of Dryden et al. (2009a) who, in effect, model $P^+(m)$ as a subspace of Σ_m^{m+1} . More subtly one could model as well using Kendall's *reflection size-and-shape space*. In fact, modeling within size-and-shape space is equivalent to embedding reflection size-and-shape space in size-and-shape space.

To this end consider the following canonical domain for upper triangular matrices

$$UT(m) = \left\{ a \in M(m, m) : \begin{array}{l} \text{there is } 1 \leq i_0 \leq m \text{ such that for} \\ \left. \begin{array}{l} i = 1 : \text{ there is } m \geq j_1 \geq 1 \text{ with } a_{ij_1} > 0 \text{ and } a_{il} = 0 \text{ for all } 1 \leq l < j_1, \\ 2 \leq i \leq i_0 : \text{ there is } m \geq j_i \geq j_{i-1} + 1 \text{ with } a_{il} = 0 \text{ for all } 1 \leq l < j_i, \text{ and} \\ \qquad \qquad \qquad a_{ij_i} > 0 \text{ in case } i < m, \\ i_0 < i : \text{ } a_{ij} = 0 \text{ for all } j = 1, \dots, m \end{array} \right\} \right\},$$

the sphere $SUT(m) = \{a \in UT(m) : \|a\| = 1\}$, $UT^{\geq}(m) = \{a \in UT(m) : a_{mm} \geq 0\}$ and $SUT^{\geq}(m) = SUT(m) \cap UT^{\geq}(m)$. Moreover, with a bijective extension of the Cholesky factorization, the corresponding canonical projections from Section 2: π and $s\pi$, $s(x) = \|x\|$ and bijections ϕ, ϕ_s , consider the following diagram of mappings:

$$\left. \begin{array}{ccc} P(m) & & \\ \uparrow \text{chol} & & \\ UT^{\geq}(m) & \hookrightarrow & SO(m) \times UT(m) \end{array} \begin{array}{c} \xrightarrow{(g,a) \mapsto ga} \\ \xrightarrow{(\pi,s)} \end{array} \left. \begin{array}{c} F_m^{m+1} \\ \downarrow s\pi \\ S\Sigma_m^{m+1} \\ \uparrow \phi_s \\ UT^{\geq}(m) \end{array} \right\} \begin{array}{c} \Sigma_m^{m+1} \times \mathbb{R}_+ \\ \uparrow \phi \\ SUT^{\geq}(m) \end{array} \quad (6)$$

In particular, (6) gives rise to the following mappings

$$\tau_s : P(m) \rightarrow S\Sigma_m^{m+1} \text{ and } \tau : P(m) \rightarrow \Sigma_m^{m+1}.$$

Theorem 5.1. *The mappings τ_s and τ are well defined, open and continuous. Moreover*

- (i) τ_s restricted to the space of mildly rank-deficient diffusion tensors $P^*(m)$ is an injective mapping into the manifold part $(S\Sigma_m^{m+1})^*$ of Kendall's size-and-shape space. Restricted to the space of full rank diffusion tensors it is a diffeomorphism onto an open subset.
- (ii) τ restricted to the space of mildly rank-deficient diffusion tensors $P^*(m)$ maps into the manifold part $(\Sigma_m^{m+1})^*$. Restricted to the space of full rank diffusion tensors it is a submersion of codimension 1 onto an open subset.

For the proof of Theorem 5.1 and diagram (6) we refer to the appendix.

Remark 5.2. *In consequence, inference for mildly deficient-rank diffusion tensors can be carried out via τ_s or τ utilizing the CLT: Theorem 3.7. Moreover, mean shapes can be pulled back under $(\tau_s)^{-1}$ to obtain mean diffusion tensors if they stay away from the region corresponding to $a_{mm} < 0$ in $UT(m)$.*

5.2 Perturbation Inconsistency for Diffusion Tensors

A typical perturbation model considered by Dryden et al. (2009a) is

$$x_i = (\mu + \epsilon_i)^T(\mu + \epsilon_i) \quad (7)$$

with perturbation mean $\mu \in UT(m)$ and error ϵ_i following a Gaussian distribution $\mathcal{N}(0, \sigma^2)$ independently in every component or in every upper diagonal component and zero in every strictly lower diagonal component. In order to relate the quality of the embedding τ_s from (6) to other structures for the space of diffusion tensors (e.g. that of the universal symmetric space), Dryden et al. (2009a) compare the partial Procrustes distance between $\tau_s(\mu^T \mu)$ and partial Procrustes means from samples of (7).

For illustration we report in Table 2 a simulation in analogy to Section 4.1 (using partial Procrustes means instead of full Procrustes means, cf. Table 1) for three typical diffusion tensors for upper triangular isotropic errors. The situation is similar for isotropic errors. The values of $\hat{d}^{(n,N)}$ for $\sigma = 0.1$ in our Table 2 correspond to the ‘‘RMSE(d_S) of $\hat{\Sigma}_S$ ’’ reported in the blocks labelled ‘‘II’’ in ‘‘Table 2’’ (corresponding to our second block) and ‘‘Table 3’’ (corresponding to our third block) of Dryden et al. (2009a). Here, however, we used $n = 10,000$ and identified these numbers as a measure only for perturbation inconsistency by additionally computing the standard error. We remark the consequence.

Remark 5.3. *Suppose that X follows a perturbation model (7). For upper triangular perturbation mean μ and error ϵ this is an anisotropic perturbation model for $S\Sigma_m^{m+1}$. For ϵ independent Gaussian in every component, $\mathbb{E}(\text{chol}(X)) \neq \text{chol}(\mu)$ in general (cf. Lemma A.2 in the appendix). Simulations corroborate inconsistency with the geometry of $S\Sigma_3^k$. Surprisingly it seems that incompatibility is not increasing, near degeneracy. This observation may be taken as an explanation for successful modeling of nearly rank deficient diffusion tensors via Kendall's size-and-shape spaces and certainly deserves further research.*

μ	σ	$\hat{d}^{(n,N)}$	$\hat{\sigma}^{(n,N)}$
$\begin{pmatrix} 1 & 0 & 0 \\ 0 & 1 & 0 \\ 0 & 0 & 1 \end{pmatrix}$	0.1	0.12	0.0017
	0.01	0.012	0.00017
	0.001	0.0012	$1.6e - 05$
$\begin{pmatrix} 1 & 0 & 0 \\ 0 & 0.3 & 0 \\ 0 & 0 & 0.1 \end{pmatrix}$	0.1	0.023	0.0020
	0.01	0.00026	0.00023
	0.001	$2.4e - 05$	$2.5e - 05$
$\begin{pmatrix} 1 & 0 & 0 \\ 0 & 0.01 & 0 \\ 0 & 0 & 0 \end{pmatrix}$	0.1	0.14	0.0019
	0.01	0.0085	0.00021
	0.001	0.00081	$2.2 - 05$

Table 2: Estimated distance $\hat{d}^{(n,N)}$ between size-and-shape of μ from the perturbation model (7) and corresponding partial Procrustes mean with standard error $\hat{\sigma}^{(n,N)}$ for $n = 10,000$ and $N = 10$. The error follows independently $\mathcal{N}(0, \sigma^2)$ in every upper triangular component.

6 Assessing Tree Bole Cylindricity

We conclude with an application from forest biometry. As basic descriptors for the shape of tree boles, *taper curves* relate height above ground level with the area of a cross section at that height. The shape of a tree stem is thus described by a two-dimensional curve. Empirical curves can be directly analyzed with methods of shape analysis, e.g. Krepela (2002) or, sophisticated models based on biological and elastomechanical context can be sought for, e.g. Chiba and Shinozaki (1994) or Gaffrey et al. (1998). For a discussion of current taper curve models cf. Li and Weiskittel (2010). While taper curves, following Cavalieri’s principle, model tree stems by *circular frusta*, recently bole ellipticality has been studied more closely, e.g. Skatter and Hoibo (1998) or Koizumi and Hirai (2006). In particular, Rappold et al. (2007) model 3D logs by *elliptical frusta* and discuss the impact of their findings on commercial logging: proximity to circular frusta increases the volume produced and reduces the number of turns to reposition logs in sawing machines and thus the total sawing time.

6.1 Data Description

Usually, tree stems are divided into three different parts: a short neiloid bottom part with strong tapering connecting with the root system, the main bole with little tapering – which is of prime commercial interest – and a conical top (e.g. Li and Weiskittel (2010)). Typically a *butt log* that is a frustum taken above *breast height* (1.3 m) is used to assess bole quality. For our application, we use 1 m butt logs from five Douglas fir trees typical for the inside of a small experimental stand in the Netherlands as detailed by Gaffrey and Sloboda (2001). At about the age of 10 to 15 years, tree crowns met; subsequently with almost no thinning, competition for light increased strongly. The entire ring structure of

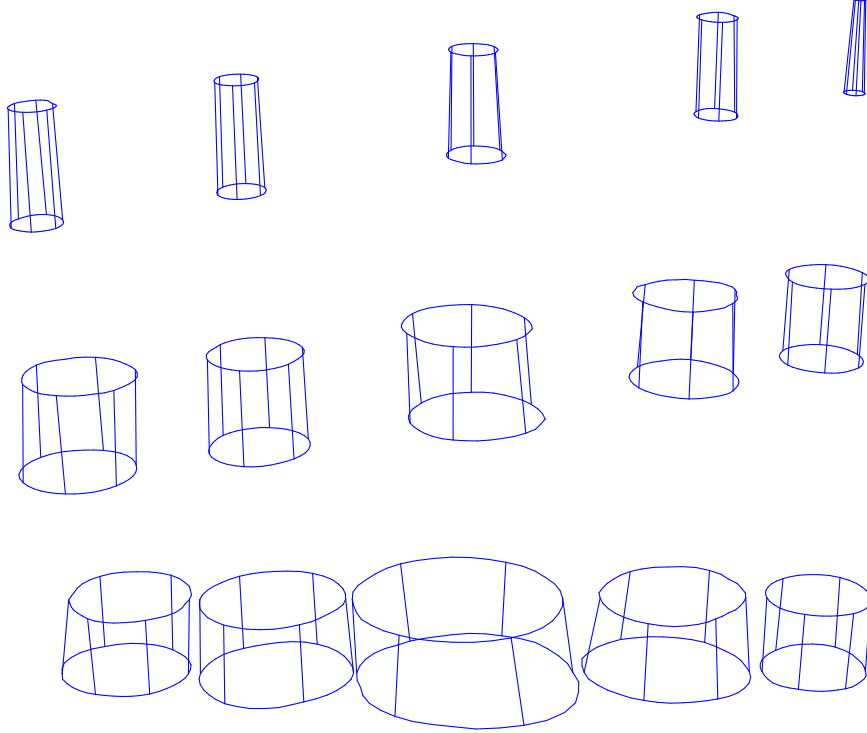


Figure 3: *Distorted view (the center frustum in the bottom row has a diameter of approx. 50 cm) along 36 angles of 1 m butt logs of five Douglas firs at ages 8 years (top row), 30 years (middle row) and 62 years (bottom row).*

bottom and top disk has been elaborately reconstructed along 36 equally spaced angles allowing to reconstruct the butt logs for every age beginning from 8 years to 62 years as displayed in Figure 3 for early, intermediate and ultimate age.

6.2 Elliptical-Like Frusta: A Totally Geodesic Subspace

In order to assess the deviation of a 1 m frustum from a cylinder (of unknown dimensions), we compute the shape distance to the space of all cylinders. To this end, and in order to compare with a model building on elliptical frusta, we introduce a suitable subspace of configurations and shapes.

For given $\mathbf{a}^T, \mathbf{b}^T, \mathbf{1}^T = (1, \dots, 1)^T \in \mathbb{R}^k$ with

$$\langle \mathbf{a}, \mathbf{b} \rangle = 0 = \langle \mathbf{a}, \mathbf{1} \rangle = \langle \mathbf{b}, \mathbf{1} \rangle \quad (8)$$

and $r, \alpha, t > 0$ let

$$w_{\alpha, \beta, r, t} := \begin{pmatrix} r \mathbf{a} & rt \mathbf{a} \\ r\alpha \mathbf{b} & r\beta t \mathbf{b} \\ 0 \mathbf{1} & \mathbf{1} \end{pmatrix}$$

be the configuration of an *elliptical-like* unit height frustum. In case of $\mathbf{a} = (\cos(2\pi/\kappa), \dots, \cos(2\pi\kappa/\kappa))$ and $\mathbf{b} = (\sin(2\pi/\kappa), \dots, \sin(2\pi\kappa/\kappa))$ we have an *elliptical* frustum of mean radius r , tapering t with bottom half axes of length $r, r\alpha$ and top half axes of length $tr, tr\beta$. A *straight frustum* has $t = 1$, a *circular frustum* has $\alpha = 1 = \beta$ and a *cylinder* is a straight circular frustum. On the grounds of the findings of Chiba and Shinozaki (1994), that for a large middle part of the bole, there is little shape variation when moving upward, a possible torsion between top and bottom ellipse is neglected in this model. Denote by

$$PS_{\mathbf{a}, \mathbf{b}} := \left\{ \frac{w}{\|w\|} : w \in P_{\mathbf{a}, \mathbf{b}} \right\} \subset S_3^{2\kappa}$$

the pre-shapes of all *elliptical-like frusta* determined by $\mathbf{a}, \mathbf{b} \in \mathbb{R}^\kappa$ satisfying (8). Here

$$P_{\mathbf{a}, \mathbf{b}} := \{w_{\alpha, \beta, r, t} \mathcal{H} : \alpha, \beta, r, t > 0\} \subset F_3^{2\kappa}$$

and \mathcal{H} denotes the Helmert sub-matrix from (1) in Section 2.

Recall that a submanifold $P \subset M$ is *totally geodesic* if for any two points in P any minimal geodesic segment joining the two in M is contained in P .

Theorem 6.1. *Consider $\mathbf{a}^T, \mathbf{b}^T \in \mathbb{R}^\kappa$ satisfying (8). Then the shapes of all elliptical-like frusta form a totally geodesic submanifold of $(\Sigma_3^{2\kappa})^*$ with horizontal lift $PS_{\mathbf{a}, \mathbf{b}}$ to $S_3^{2\kappa}$.*

The proof of Theorem 6.1 is found in the appendix. We have at once:

Corollary 6.2. *The shapes of cylinders form a segment on a geodesic in $(\Sigma_3^{2\kappa})^*$.*

6.3 Data Analysis

The distance of the shape of a frustum to the geodesic spanned by the shapes of cylinders is computed via a method proposed in Huckemann et al. (2010). Since for every age considered there are only five frusta, a 95% confidence band for the distance of the full Procrustes mean to the geodesic of cylinders has been computed by 200 Bootstrap resamples. As clearly visible in Figure 4, young frusta until the age of approx. 15 years tend to toward cylinders. At later ages they tend away again. The change point at approx. 15 years can be explained by the fact that at this time competition for light began.

Note that uniform growth naturally decreases tapering and ellipticity. In order to compare the initial growth to uniform growth, three curves of elliptical frusta starting with t and $\alpha = \beta$ in the range of corresponding estimated butt log values as well as with size growth identical to the mean size growth are

depicted in the left display of Figure 4 (95 % of estimated tapering coefficients t observed are between 0.864 and 0.986; a crude estimate for α and β gives 95 % of observed values between 1.02 and 1.13 (after rotating such that $\alpha, \beta \geq 1$)). This comparison yields that observed initial growth towards cylinders appears even stronger than uniform.

In order to assess the growth of the older logs, compare it to the growth of elliptical frusta keeping tapering and ellipticity constant while letting size grow with the mean size of the original data. Three of such curves are depicted in the right display of Figure 4. The observed movement away from the geodesics of cylinders appears rather similar.

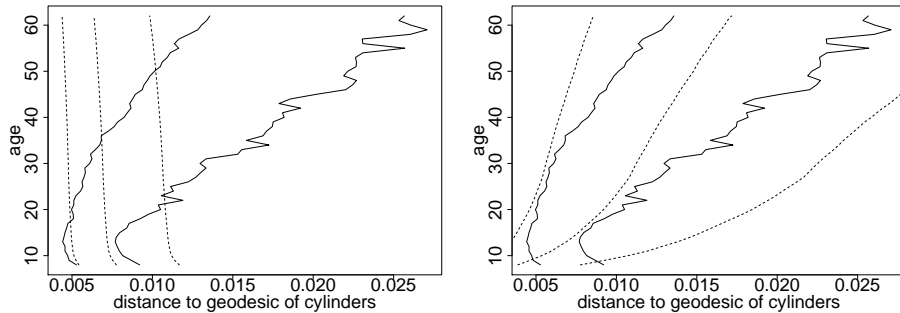


Figure 4: *Solid: confidence band for the distance of the Procrustes mean shape of 1 m butt logs above breast height to the geodesic of cylinders for each year based on 200 bootstrapped Procrustes means. For comparison dashed: uniform equalsize growth of elliptical cylinders (left display) starting with $(\alpha = \beta, t) = (1.07, 0.93), (1.1, 0.9), (1.15, 0.85)$ from left to right; equalsize growth of elliptical cylinders (right display) with constant $(\alpha = \beta, t) = (1.025, 0.975), (1.05, 0.95), (1.1, 0.9)$ from left to right.*

Summarizing, this study indicates that tree boles of young Douglas fir trees with little competition grow uniformly or even stronger towards cylinders. Older tree boles their crowns competing for light, grow as if they keep ellipticity and tapering constant. These findings certainly call for more elaborate research, e.g. tapering and ellipticity can be investigated by developing a method to study distance and projection to the submanifold of elliptical-like frusta.

7 Conclusion and Outlook

In this paper for the statistical analysis of 3D shape, an asymptotic result for mean shape has been derived, a classical perturbation model and a newly proposed perturbation model for the statistical analysis of diffusion tensors has been revisited, and inference on the temporal deviation of the 3D shape of tree boles from cylinders has been performed.

Although Procrustes means are very popular, it seems that due to a misunderstanding, the notion of 3D *Procrustes population means* had not been quite available in the community. Instead, population means of a perturbation model had been estimated by *Procrustes sample means* which were, as was well known, “consistent” estimators under isotropic 2D errors. Introducing Fréchet ρ -means in this work and extending the available Central-Limit Theorem to underlying non-metrical distances, in particular, the issue of “consistency” has been identified as an “incompatibility” of the perturbation model with the shape space’s geometry. Moreover, we recalled a Fréchet ρ -mean introduced by Ziezold (1994) the computation of which in 3D is computationally slightly less costly than the computation of Procrustes means. This result allows for one-sample tests for a population Procrustes or Ziezold mean on the manifold part of the shape space, since due to strong consistency, sample Procrustes or Ziezold means will eventually come to lie on the manifold part a.s. For a two-sample test, one would need to ensure that Procrustes and Ziezold means are contained on the manifold part, if the underlying random shapes are a.s. contained in the manifold part. Settling this issue is the subject of a separate research, cf. Huckemann (2010).

While many means, different from classical intrinsic, extrinsic or Procrustes means are Fréchet ρ -means (e.g. geometric medians of Fletcher et al. (2008) and (penalized) weighted Procrustes means of Dryden et al. (2009b)) it would be interesting to verify whether a larger class of means, e.g. the semi-metrical mean introduced in Schmidt et al. (2007) and successfully employed in computer vision also fall into this setup.

Within the discussion of “consistency”, the modeling of Dryden et al. (2009a) for diffusion tensor imaging has been extended to diffusion tensors mildly deficient in rank. To the knowledge of the author, this is the first framework allowing for statistical inference on non-regular diffusion tensors without utilizing a Euclidean embedding, say, in the space of symmetric matrices. Of course in many applications, the interest lies specifically in degenerate tensors because these indicate a strong directional flow. The finding that mildly rank-deficient diffusion tensors are only “mildly perturbation inconsistent” may provide for another motivation for the approach of Dryden et al. (2009a,b). Following Dryden et al. (2009a), we have used Procrustes means. For the underlying reflection shape space, extrinsic Schoenberg means qualify as well, they compute much faster than Procrustes or Ziezold means. As the most important advantage, the two-sample tests of Bhattacharya (2008) can then be performed even including rank 1 diffusion tensors. A drawback, however, may result from a possible insensitivity of Schoenberg means to degeneracy thus yielding a smaller discrimination power (cf. Huckemann (2010) for a detailed discussion). These issues certainly warrant further research.

Briefly compiling the findings on tree boles we can add to the well known fact that longest boles can be found in dense stands, it seems that the most cylindrical boles can be found in young stands with low competition.

A geodesic perturbation model. As demonstrated in this work, for most practical applications in 3D avoiding degenerate configurations, perturbation

models may be considered compatible with the shape space’s geometry for isotropic error. Note that the shapes of entire tree boles are nearly singular (cf. Huckemann et al. (2010)). For short bole frusta, however, such models may still serve intuition and for sufficiently small error provide an adequate approximation. As one of such consider the *geodesic perturbation model*

$$x_i = g_i \lambda_i (\gamma(s_i) + \epsilon_i) \quad (9)$$

with a straight line $s \rightarrow \gamma(s) = \mu + s\nu$ in configuration space F_m^k such that locally all points on γ are in optimal position to each other. For 3D frusta, the geodesic of cylinders has been used here, any other geodesic of specific frusta can be used similarly. Moreover, based on larger samples, a geodesic perturbation model within the space of elliptical-like frusta can be used to assess specific model parameters. In particular, a close investigation of such model parameters may lead to inference on the impact of environmental effects on the shape of tree boles building on artificially induced modifications of biological tree parameters as in Gaffrey and Sloboda (2004).

Acknowledgments: The author would like to express his sincerest gratitude to the late Herbert Ziezold (1942 – 2008) whose untimely death was most unfortunate. He would also like to thank Dieter Gaffrey and the colleagues from the Institute for Forest Biometry and Informatics at the University of Göttingen for discussion of and supplying with the tree-bole data. Also he is grateful for helpful discussions with Thomas Hotz, John Kent and Axel Munk.

A Appendix: Proofs

The Central-Limit-Theorem for Fréchet ρ -means. With the notation of Section 3.2, suppose that $\rho : Q \times P \rightarrow [0, \infty)$ is a map, ρ^2 smooth in the second component as specified below. In a local chart (ϕ, U) of P near $\phi^{-1}(0) \in P$, denote by $\text{grad}_2 \rho(q, p)^2$ the gradient of $x \mapsto \rho(q, \phi^{-1}(x))^2$ and by $H_2 \rho(q, p)^2$ the corresponding Hessian matrix of second order derivatives. Then similar to Bhattacharya and Patrangenaru (2005, p.1230) consider the following integrability condition on a random variable X on Q at a location $\mu \in P$:

$$\left. \begin{array}{ll} \mathbb{E}(\text{grad}_2 \rho(X, \mu)^2) & \text{exists,} \\ \text{COV}(\text{grad}_2 \rho(X, \mu)^2) & \text{exists,} \\ \mathbb{E}(H_2 \rho(X, \nu)^2) & \text{exists for } \nu \text{ near } \mu \text{ and is continuous at } \nu = \mu. \end{array} \right\} (10)$$

In analogy to condition (3) consider

$$\exists \epsilon > 0 \quad \text{such that} \quad x \mapsto \rho(X, \phi^{-1}(x))^2 \text{ is smooth for } |x| < \epsilon \text{ a.s.} \quad (11)$$

The validity of (10) and (11) is independent of the particular chart chosen. If ρ is the Euclidean distance or $\rho = d_{S\Sigma_m^k}^{(i)}$, then (10) is valid if $\mathbb{E}(\|X\|^2) < \infty$.

If there is a discrete group H acting on P and $\mu \in P$ such that $E^{(\rho)} = \{h\mu : h \in H\}$, we say that the Fréchet population ρ -mean set is *unique up to the action of H* .

Theorem A.1. *Suppose that μ is a point in the Fréchet ρ -mean set unique up to the action of H on a manifold P with respect to a continuous function $\rho : Q \times P \rightarrow \mathbb{R}$, ρ^2 smooth in the second component in the sense of (11), satisfying strong consistency, where Q is a topological space. If*

for any measurable choice $p_n \in E_n^{(\rho)}$ there is a sequence $h_n \in H$ such that $\mu_n = h_n p_n \rightarrow \mu$ a.s., and if

- (i) X has compact support or*
- (ii) the integrability conditions (10) are satisfied at μ*

then for any measurable choice $p_n \in E_n^{(\rho)}$ there is a sequence $h_n \in H$ such that $\mu_n = h_n p_n$ satisfies a CLT. In a suitable chart (ϕ, U) the corresponding matrices from Definition 3.6 are given by

$$A = \mathbb{E}(H_2\rho(X, \mu)^2), \quad \Sigma = \text{COV}(\text{grad}_2 \rho(X, \mu)^2).$$

Proof. Obviously, if X has compact support then (10) is satisfied. Hence we may assume the case (ii). We adapt the ideas laid out in Bhattacharya and Patrangenaru (2005, p. 1229–1230). Let D denote the dimension of P and consider a local chart (U, ϕ) near $\mu = \phi^{-1}(0)$. We have a.s. eventually that $\mu_n \in U$, then $\phi(\mu_n) = x_n \rightarrow 0$ a.s. Abbreviating $g(x) = \sum_{j=1}^n \rho(X_j, \phi^{-1}(x))^2$, $\text{grad } g(x) = (g_1(x), \dots, g_D(x))^T$ and $Hg(x)$ for the Hessian we have by (11) the Taylor expansion

$$\begin{aligned} 0 &= \frac{1}{\sqrt{n}} \text{grad } g(x_n) = \frac{1}{\sqrt{n}} \text{grad } g(0) + \frac{1}{\sqrt{n}} \begin{pmatrix} (\text{grad } g_1(t_1 x_n))^T \cdot x_n \\ \vdots \\ (\text{grad } g_D(t_D x_n))^T \cdot x_n \end{pmatrix} \\ &= \frac{1}{\sqrt{n}} \text{grad } g(0) + \frac{1}{n} Hg(0) \cdot \sqrt{n} x_n + \frac{1}{n} \begin{pmatrix} (\text{grad } g_1(t_1 x_n) - \text{grad } g_1(0))^T \cdot \sqrt{n} x_n \\ \vdots \\ (\text{grad } g_D(t_D x_n) - \text{grad } g_D(0))^T \cdot \sqrt{n} x_n \end{pmatrix} \end{aligned}$$

for suitable $0 \leq t_1, \dots, t_D \leq 1$ a.s. In conjunction with the classical CLT, the first two conditions in (10) ensure that

$$\frac{1}{\sqrt{n}} \text{grad } g(0) = \frac{1}{\sqrt{n}} \sum_{j=1}^n \text{grad}_2 \rho(X_j, \phi^{-1}(0))^2 \rightarrow -\mathcal{G}$$

in distribution for some Gaussian matrix \mathcal{G} with mean $\mathbb{E}(\text{grad}_2 \rho(X, \phi^{-1}(0))^2) = 0$ and covariance matrix $\text{COV}(\text{grad}_2 \rho(X, \phi^{-1}(0))^2)$. The third condition guarantees the Strong Law of Large Numbers for the mean of random Hessians

$$\frac{1}{n} Hg(0) = \frac{1}{n} \sum_{j=1}^n H_2\rho(X_j, \phi^{-1}(0))^2 \rightarrow \mathbb{E}(H_2\rho(X, \mu)^2) =: A \text{ a.s.}$$

Note that the k -th entry of $\frac{1}{n} (\text{grad } g_i(t_i x_n) - \text{grad } g_i(0))$ for $1 \leq i, k \leq D$ is

$$\frac{1}{n} \sum_{j=1}^n \left(\frac{\partial^2}{\partial_i \partial_k} \rho(X_j, \phi^{-1}(t_i x_n))^2 - \frac{\partial^2}{\partial_i \partial_k} \rho(X_j, \phi^{-1}(0))^2 \right)$$

which tends to zero a.s. again by the third condition of (10). In consequence $A\sqrt{n}x_n \rightarrow \mathcal{G}$ in distribution yielding the assertion. \square

Proof of Theorem 5.1. First in I we define an extension of the Cholesky factorization which yields that τ and τ_s are well defined. Then in II we show the topological properties of τ and τ_s . The other assertions of Theorem 5.1 are then straightforward.

I: Define an extension of the Cholesky factorization by $P(m) \ni a = v\lambda^2v^T \rightarrow b = \sqrt{\lambda}v^T = gu \rightarrow u \in UT^{\geq}(m)$ where λ is a diagonal matrix with non-negative entries, $v, g \in SO(m)$. Then, obviously $u^T u = a$. The factorization $b = gu$ is obtained by the usual Gram-Schmidt process, i.e. the first column g_1 of g is $b_{(1)}/\|b_{(1)}\|$ where $b_{(1)}$ denotes the first non-zero column in b , the second column is $g_2 = (b_{(2)} - g_1b_{(2)}^Tg_1)/\|b_{(2)} - g_1b_{(2)}^Tg_1\|$ with $b_{(2)}$, the first column in b linearly independent of g_1 , etc.. Either proceed until g_m (note that we have $u_{mm} \geq 0$ in consequence of $\det(b) \geq 0$ and $g \in SO(m)$) or extend with arbitrary columns such that $g \in SO(m)$. In order to see that this mapping is well defined suppose that $u' \in UT^{\geq}(m)$ and $g' \in SO(m)$ with $u'^T u' = uu^T$. Set

$$u = \begin{pmatrix} q \\ 0 \end{pmatrix}, \quad u' = \begin{pmatrix} q' \\ 0 \end{pmatrix}$$

with a matrices $q, q' \in M(r, m)$ of rank r . Then, there are indices $1 \leq j_1 \leq \dots \leq j_r$ such that the matrix $\tilde{q} = (q_{j_1}, \dots, q_{j_r})$ composed of linearly independent columns q_{j_1}, \dots, q_{j_r} of q is upper triangular and regular, i.e. $\tilde{q} \in UT^+(r)$. Denoting by $\tilde{q}' = (q'_{j_1}, \dots, q'_{j_r})$ the matrix composed of the corresponding columns of q' note that by construction $\tilde{q}' \in UT(r)$. By hypothesis, $\tilde{q}'^T \tilde{q}' = \tilde{q}^T \tilde{q}$ which yields with the classical Cholesky decomposition that $\tilde{q}' = \tilde{q}$. Since $\tilde{q}'^T \hat{q}' = \tilde{q}^T \hat{q}$ with “ $\hat{\cdot}$ ” standing for the complementary columns in $\{1, \dots, r\}$ we have indeed $q' = q$, i.e. $u' = u$. Obviously this mapping is an extension of the classical Cholesky factorization.

The bijective mappings $\phi : \Sigma_m^{m+1} \rightarrow SUT(m)$ and $\phi_s : S\Sigma_m^{m+1} \rightarrow UT(m)$ are similarly obtained (cf. Kendall et al. (1999, Section 1.3)) by a Gram-Schmidt decomposition of $a \in [a] \in S\Sigma_m^{m+1}$. To this end choose the sign of u_{mm} such that $g \in SO(m)$ which possibly gives a negative entry u_{mm} . Note that

$$\phi_s \circ \tau_s(P(n)) = UT^{\geq}(m) \quad \text{and} \quad \phi \circ \tau(P(n)) = SUT^{\geq}(m).$$

This shows that τ and τ_s are indeed well defined. Moreover, τ_s is injective.

II: We now rely on the decomposition of $UT(m)$ and $SUT(m)$ as simplicial complexes by Kendall et al. (1999, Chapter 2) defined through the topologies of $S\Sigma_m^{m+1}$ and Σ_m^{m+1} , respectively. Verify that the boundary identification on the respective subsets $UT^{\geq}(m)$ and $SUT^{\geq}(m)$ is the same as given by the natural topology of $P(m)$. Hence, τ and τ_s are both open and continuous. \square

Lemma A.2. *Let $e \in F_m^{m+1}$ be the unit matrix and $a = (e + \epsilon)^T(e + \epsilon)$ with error $\epsilon \in F_m^{m+1}$ independent standard normal in every component. Then,*

$$\mathbb{E}(\text{chol}(a)) \neq e.$$

Proof. Let $e + \delta = \text{chol}(a)$ giving for the entry in the first column and row

$$1 + \delta_{11} = \sqrt{1 + 2\epsilon_{11} + \sum_{j=1}^m \epsilon_{j1}^2}.$$

Since $\sqrt{(1+x)^2+y^2} + \sqrt{(1-x)^2+y^2} \geq 2\sqrt{x^2+y^2}$ observe that

$$\mathbb{E} \left(\sqrt{(1+\epsilon_{11})^2 + \sum_{j=2}^m \epsilon_{j1}^2} \right) \geq \mathbb{E} \left(\sqrt{\sum_{j=1}^m \epsilon_{j1}^2} \right) = \sqrt{2} \frac{\Gamma(\frac{m+1}{2})}{\Gamma(\frac{m}{2})} > 1$$

for $m > 1$. Hence $\mathbb{E}(e + \delta) = e$ cannot be. \square

Proof of Theorem 6.1. Since the diagonal of $w_{\alpha,\beta,r,t} w_{\alpha',\beta',r',t'}^T$ consists of positive values only, all elements of $PS_{\mathbf{a},\mathbf{b}}$ are mutually unique in optimal position (Kendall et al. (1999, p. 114)). Since straight lines are mapped under the Helmert sub-matrix to straight lines in the configuration space which project to great circles in the pre-shape space, the straight line segment between $w_{\alpha,\beta,r,t}$ and $w_{\alpha',\beta',r',t'}$ maps to a segment on a horizontal geodesic on S_m^k . In consequence, the projection of $PS_{\mathbf{a},\mathbf{b}}$ to $(\Sigma_3^{2\kappa})^*$ is a totally geodesic submanifold, its horizontal lift is again $PS_{\mathbf{a},\mathbf{b}}$, cf. Huckemann et al. (2010, Section 2). \square

References

- Abraham, R., Marsden, J. E., 1978. Foundations of Mechanics, 2nd Edition. Benjamin-Cummings.
- Bhattacharya, A., 2008. Statistical analysis on manifolds: A nonparametric approach for inference on shape spaces. Sankhya, Ser. A 70 (2), 223–266.
- Bhattacharya, R. N., Patrangenaru, V., 2003. Large sample theory of intrinsic and extrinsic sample means on manifolds I. Ann. Statist. 31 (1), 1–29.
- Bhattacharya, R. N., Patrangenaru, V., 2005. Large sample theory of intrinsic and extrinsic sample means on manifolds II. Ann. Statist. 33 (3), 1225–1259.
- Cao, Y., Miller, M. I., Mori, S., Winslow, R. L., Younes, L., 2006. Diffeomorphic matching of diffusion tensor images. In: Computer Vision and Pattern Recognition Workshop, 2006 Conference on. p. 67.
- Chiba, Y., Shinozaki, K., 1994. A simple mathematical model of growth pattern in tree stems. Annals of Botany 73, 91–98.
- Dryden, I., Koloydenko, A., Zhou, D., 2009a. Non-euclidean statistics for covariance matrices, with applications to diffusion tensor imaging. Annals of Applied Statistics 3 (3), 1102–1123.
- Dryden, I., Koloydenko, A., Zhou, D., Li, B., 2009b. Non-euclidean statistical analysis of covariance matrices and diffusion tensors. Proc. of the ISI2009.
- Dryden, I. L., 2009. R-package for the statistical analysis of shapes, <http://www.maths.nott.ac.uk/~ild/shapes>.
- Dryden, I. L., Mardia, K. V., 1998. Statistical Shape Analysis. Wiley, Chichester.

- Fletcher, P., Venkatasubramanian, S., Joshi, S., 2008. Robust statistics on Riemannian manifolds via the geometric median. In: *Computer Vision and Pattern Recognition, 2008. CVPR 2008. IEEE Conference on.* IEEE, pp. 1–8.
- Fletcher, P. T., Joshi, S. C., 2004. Principal geodesic analysis on symmetric spaces: Statistics of diffusion tensors. *ECCV Workshops CVAMIA and MM-BIA*, 87–98.
- Fréchet, M., 1948. Les éléments aléatoires de nature quelconque dans un espace distancié. *Ann. Inst. H. Poincaré* 10 (4), 215–310.
- Gaffrey, D., Sloboda, B., 2001. Tree mechanics, hydraulics and needle-mass distribution as a possible basis for explaining the dynamics of stem morphology. *Journal of Forest Science* 47 (6), 241–254.
- Gaffrey, D., Sloboda, B., 2004. Modifying the elastomechanics of the stem and the crown needle mass distribution to affect the diameter increment distribution: A field experiment on 20-year old abies grandis trees. *Journal of Forest Science* 50 (5), 199–210.
- Gaffrey, D., Sloboda, B., Matsumura, N., 1998. Representation of tree stem taper curves and their dynamic, using a linear model and the centroaffine transformation. *J. For. Res.* 3, 67–74.
- Goodall, C. R., 1991. Procrustes methods in the statistical analysis of shape (with discussion). *Journal of the Royal Statistical Society, Series B* 53, 285–339.
- Gower, J. C., 1975. Generalized Procrustes analysis. *Psychometrika* 40, 33–51.
- Grossier, D., 2005. On the convergence of some Procrustean averaging algorithms. *Stochastics: Internatl. J. Probab. Stochastic. Processes* 77 (1), 51–60.
- Huckemann, S., 2010. On the meaning of mean shape. Preprint, arXiv, 1002.0795v1 [stat.ME].
- Huckemann, S., Hotz, T., Munk, A., 2010. Intrinsic shape analysis: Geodesic principal component analysis for Riemannian manifolds modulo Lie group actions (with discussion). *Statistica Sinica* 20 (1), 1–100.
- Kendall, D. G., 1977. The diffusion of shape. *Adv. Appl. Prob.* 9, 428–430.
- Kendall, D. G., 1984. Shape manifolds, Procrustean metrics and complex projective spaces. *Bull. Lond. Math. Soc.* 16 (2), 81–121.
- Kendall, D. G., Barden, D., Carne, T. K., Le, H., 1999. *Shape and Shape Theory*. Wiley, Chichester.
- Kent, J. T., Mardia, K. V., 1997. Consistency of Procrustes estimators. *Journal of the Royal Statistical Society, Series B* 59 (1), 281–290.

- Koizumi, A., Hirai, T., 2006. Evaluation of the section modulus for tree-stem cross sections of irregular shape. *Journal of Wood Science* 52 (3), 213–219.
- Krepela, M., 2002. Point distribution form model for spruce stems (*picea abies* [l.] karst.). *Journal of Forest Science* 48 (4), 150–155.
- Lang, S., 1999. *Fundamentals of Differential Geometry*. Springer.
- Le, H., 1998. On the consistency of Procrustean mean shapes. *Adv. Appl. Prob. (SGSA)* 30 (1), 53–63.
- Le, H., 2001. Locating Fréchet means with an application to shape spaces. *Adv. Appl. Prob. (SGSA)* 33 (2), 324–338.
- Lele, S., Jul. 1993. Euclidean distance matrix analysis (EDMA): estimation of mean form and mean form difference. *Math. Geol.* 25 (5), 573–602.
- Li, R., Weiskittel, A. R., 2010. Comparison of model forms for estimating stem taper and volume in the primary conifer species of the north american acadian region. *Ann. For. Sci.* 67 (3), 302.
- Mardia, K. V., Jupp, P. E., 2000. *Directional Statistics*. Wiley, New York.
- Pajevic, S., Bassler, P. J., 2003. Parametric and non-parametric statistical analysis of DT-MRI. *Journal of Magnetic Resonance* 161 (2), 1–14.
- Rappold, P. M., Bond, B. H., Wiedenbeck, J. K., Etame, R. E., 2007. Impact of elliptical shaped red oak logs on lumber grade and volume recovery. *Forest Products Journal* 57 (6), 70–73.
- Schmidt, F. R., Töppe, E., Cremers, D., Boykov, Y., 2007. Intrinsic mean for semi-metrical shape retrieval via graph cuts. In: Hamprecht, F. A., Schnörr, C., Jähne, B. (Eds.), *DAGM-Symposium*. Vol. 4713 of *Lecture Notes in Computer Science*. Springer, pp. 446–455.
- Skatter, S., Hoibo, O. A., 1998. Cross-sectional shape models of Scots Pine (*Pinus silvestris*) and Norway Spruce (*Picea abies*). *Holz als Roh-und Werkst.*, 187–191.
- Vilanova, A., Zhang, S., Kindlmann, G., Laidlaw, D., 2006. An introduction to visualization of diffusion tensor imaging and its applications. In: Weickert (Ed.), *Visualization and Processing of Tensor Fields*. Springer-Verlag, pp. 121–153.
- Ziezold, H., 1977. Expected figures and a strong law of large numbers for random elements in quasi-metric spaces. *Trans. 7th Prague Conf. Inf. Theory, Stat. Dec. Func., Random Processes A*, 591–602.
- Ziezold, H., 1994. Mean figures and mean shapes applied to biological figure and shape distributions in the plane. *Biom. J.* (36), 491–510.